Neuron, Vol. 33, 47–61, January 3, 2002, Copyright ©2002 by Cell Press

Regulation of Cortical Dendrite Development by Slit-Robo Interactions

Kristin L. Whitford,[1] Valérie Marillat,[2] Elke Stein,[3] Corey S. Goodman,[4] Marc Tessier-Lavigne,[3] Alain Chédotal,[2] and Anirvan Ghosh[1,5]
[1]Department of Neuroscience
Johns Hopkins University School of Medicine
725 N. Wolfe Street
Baltimore, Maryland 21205
[2]Institut de la Santé et de le Recherche Médicale U106
Bâtiment de Pédiatrie
Hôpital de la Salpêtrière
47 Boulevard de l'Hôpital
75013 Paris
France
[3]Howard Hughes Medical Institute
Department of Anatomy
Department of Biochemistry and Biophysics
University of California, San Francisco
San Francisco, California 94143
[4]Howard Hughes Medical Institute
Department of Molecular and Cell Biology
University of California, Berkeley
Berkeley, California 94720

Summary

Slit proteins have previously been shown to regulate axon guidance, branching, and neural migration. Here we report that, in addition to acting as a chemorepellant for cortical axons, Slit1 regulates dendritic development. Slit1 is expressed in the developing cortex, and exposure to Slit1 leads to increased dendritic growth and branching. Conversely, inhibition of Slit-Robo interactions by Robo-Fc fusion proteins or by a dominant-negative Robo attenuates dendritic branching. Stimulation of neurons transfected with a Met-Robo chimeric receptor with Hepatocyte growth factor leads to a robust induction of dendritic growth and branching, suggesting that Robo-mediated signaling is sufficient to induce dendritic remodeling. These experiments indicate that Slit-Robo interactions may exert a significant influence over the specification of cortical neuron morphology by regulating both axon guidance and dendritic patterning.

Introduction

In the vertebrate cerebral cortex, neurons are born and undergo their final mitoses in the ventricular zone, after which they migrate into the cortical plate and assume their final laminar positions. These cells are then faced with the challenge of differentiating into functioning neurons with appropriate synaptic connections. In response to local extracellular cues, these neurons initially extend an axon away from the pial surface and down toward the white matter. Once the axons arrive at the white matter, other axon guidance cues direct them toward appropriate targets, such as the thalamus, the spinal cord, or the contralateral cortex. Likewise, the apical dendrites of pyramidal cells require directional information to grow toward the pia, in the direction opposite the axons. After the initial polarity of a neuron is established, several primary dendrites emerge from the cell body, which subsequently undergo extensive growth and branching. At the same time, the apical dendrite sends out collateral branches that serve as major synaptic sites. This process allows neurons to achieve their mature morphology and to receive input from afferent axons.

In previous work directed at characterizing signals that regulate patterning of axons and dendrites in the cortex, we demonstrated the presence of a soluble axon chemorepellant activity concentrated near the pial surface of the developing cortical plate (Polleux et al., 1998). We hypothesized that once a postmitotic neuron has reached its final location in the cortical plate, this cue directs initial axonal projections away from the pia and down toward the white matter. We determined that the secreted semaphorin Sema3A, which is expressed at high levels in the cortical plate, is capable of repelling cortical axons and is a component of this activity (Polleux et al., 1998). We also found that Sema3A acts as a chemoattractant for apical dendrites, indicating that chemotropic cues can differentially influence axonal and dendritic patterning within the same neuron (Polleux et al., 2000).

While mice with a targeted deletion in Sema3A have axonal and dendritic defects, many of the cortical neurons are able to extend axons to subcortical targets, suggesting the involvement of additional axon guidance molecules. In addition, the fact that Sema3A exerts distinct effects on axons and dendrites raises the possibility that other chemotropic molecules might also have the ability to differentially influence axonal and dendritic growth. To investigate these issues, we examined the effects of other chemotropic molecules on cortical neuron development. Other than Semaphorins, the two major families of diffusible chemotropic cues are Netrins and Slits. The role of Netrins on cortical development has been previously explored, and it has been shown that Netrin1 can act as a chemoattractant for cortical axons (Metin et al., 1997; Richards et al., 1997; Serafini et al., 1996). Expression of Netrin 1 is low in the cortical plate, making it unlikely that it exerts a significant effect on dendritic specification. The Slits, in contrast, are expressed at high levels in the developing cortex, and this study focuses on the role of Slit-mediated interactions in the patterning of cortical axons and dendrites.

Slits are a family of large, secreted proteins containing four leucine-rich repeats, nine (or seven, for *Drosophila*) EGF-like repeats, a laminin-G (or ALPS or LNS) domain, and a cysteine-rich C-terminal motif (Itoh et al., 1998; Rothberg and Artavanis-Tsakonas, 1992; Rothberg et al., 1990). In the *Drosophila* nervous system, dSlit is produced by midline glial cells and functions as a chemorepellant to prevent the recrossing of commissural ax-

[5]Correspondence: aghosh@jhmi.edu

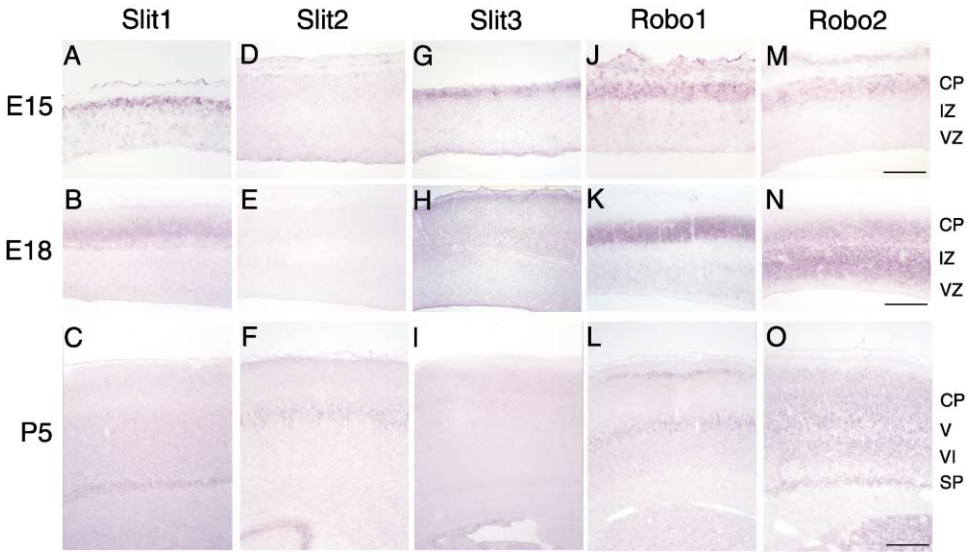

Figure 1. Embryonic and Early Postnatal Expression of *slit* and *robo* Genes in the Cortex

Examples of rat E15 and E18 sagittal sections and P5 coronal sections processed for in situ hybridization with probes for *slit1* (A–C), *slit2* (D–F), *slit3* (G–I), *robo1* (J–L), and *robo2* (M–O). The scale bars equal 200 μm in A, B, D, E, G, H, J, K, M, and N and 350 μm in C, F, I, L, and O. Abbreviations are as follows: CP, cortical plate; IZ, intermediate zone; VZ, ventricular zone; and SP, subplate.

ons (Kidd et al., 1999). This effect is mediated by the Roundabout, or Robo, family of receptors, which contain five Ig domains, three fibronectin type III (FNIII) repeats, a single transmembrane domain, and an intracellular domain with a number of conserved cytoplasmic motifs (CCO-CC3) (Kidd et al., 1998). In *Drosophila*, dSlit also controls the positioning of longitudinal axon bundles through the expression of different combinations of Robo receptors (Rajagopalan et al., 2000; Simpson et al., 2000a) and acts as a repellent for muscle precursors leaving the midline (Kidd et al., 1999). Interestingly, recent work has shown that dSlit also has a positive role in *Drosophila*; in a matter of a few hours, these migrating cells switch their responsiveness to dSlit such that muscle-insertion sites expressing dSlit become attractive for muscle cells expressing the Robo receptor (Kramer et al., 2001).

There are three vertebrate *slit* genes and three *robo* receptors (Brose et al., 1999; Yuan et al., 1999). At the vertebrate midline, there is evidence that expression of Slits and Robos controls the crossing of commisural axons in the spinal cord (Zou et al., 2000), retinal ganglion cell axons at the optic chiasm (Erskine et al., 2000; Fricke et al., 2001; Niclou et al., 2000), and fibers of the corpus callosum (Shu and Richards, 2001). Additionally, Slit1 and Slit2 expressed in the septum appear to repel olfactory bulb axons as they project into the lateral olfactory tract (Li et al., 1999; Nguyen Ba-Charvet et al., 1999). Slits also influence axon guidance outside the midline, as Slit2 is a chemorepellant for dentate gyrus axons and may prevent their invasion of the entorhinal cortex (Nguyen Ba-Charvet et al., 1999).

Along with their roles in axon repulsion, Slit proteins have been implicated in controlling axon branching. Slit2 was biochemically isolated as a branching factor for dorsal root ganglion axons (Wang et al., 1999). Interestingly, the branching activity was found to reside in a large amino-terminal fragment, Slit2-N, arising from endogenous cleavage of Slit2 between the fifth and sixth EGF repeats of the molecule, whereas full-length Slit2 does not possess this activity (Wang et al., 1999). By contrast, both full-length Slit2 and Slit2-N possess repulsive activity for axons (Nguyen Ba-Charvet et al., 2001). Whether a Robo receptor also mediates this branching effect is not known.

The role of Slits in axonal and dendritic patterning in the mammalian brain is largely unexplored. Here we report that the Slits and Robos are expressed widely and dynamically in the developing cerebral cortex. At late embryonic stages, when neurons in the cortical plate are extending axons and elaborating dendritic trees, Slit1, but not Slit2 or Slit3, is expressed at high levels, along with Robo1 and Robo2. The expression pattern of Slit1, coupled with the ability of Slit1 to repel cortical axons in an in vitro assay, suggests that Slit1 might function as the Sema3A-independent cortical-repellant factor. We also find that Slit1 exerts a major influence on dendritic growth and branching. Studies with truncated and chimeric receptors suggest that Slit1 is an endogenous dendritic branching factor and that this effect is mediated through the Robo receptors. Based on these observations, we propose that Slit1 is a bifunctional cue for cortical neurons that can differentially regulate axonal and dendritic patterning.

Results

Expression of *slit* Genes in the Developing Cortex

To determine the expression patterns of the *slit* family members in the developing rat cortex, we performed in situ hybridizations at several developmental ages. As early as embryonic day 15 (E15), when the deep layer neurons have just completed their migration and are beginning to extend axons toward the intermediate

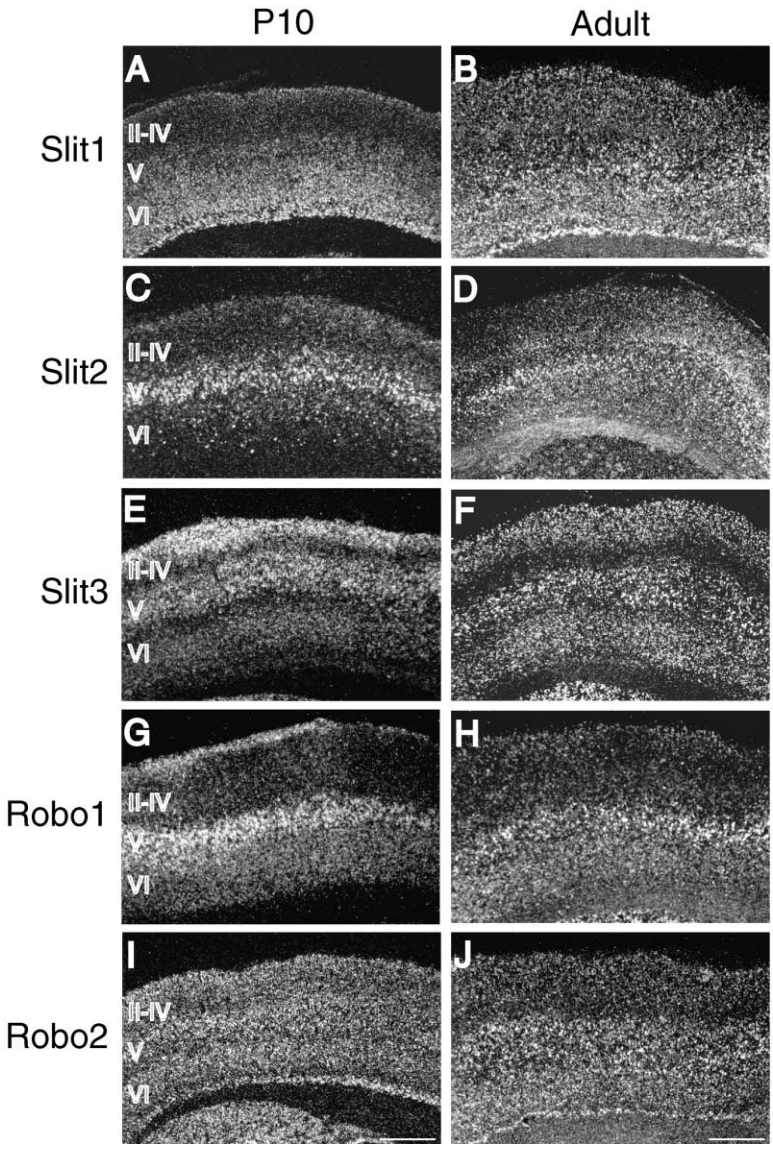

Figure 2. Later Postnatal and Adult Expression of *slit* and *robo* Genes in the Cortex

Examples of rat P10 (A, C, E, G, and I) and adult (B, D, F, H, and J) coronal sections processed for in situ hybridization with probes for *slit1* (A and B), *slit2* (C and D), *slit3* (E and F), *robo1* (G and H), and *robo2* (I and J). The scale bars equal 650 μm in (A), (C), (E), (G), and (I) and 750 μm in (B), (D), (F), (H), and (J).

zone, *slit1* is heavily expressed in the cortical plate (Figure 1A). High levels of expression throughout the cortical plate are maintained at E18 (Figure 1B) and E20 (data not shown). However, by postnatal day 1 (P1), only the infragranular layers (V and VI) and not the dense cortical plate which differentiates into layers II/III expressed *slit1* (data not shown). At P5, expression is restricted to layers V, VI, and the subplate (Figure 1C). *slit1* continues to be expressed in the adult, with highest expression in the deep cortical layers (Figure 2B).

slit2 is not expressed in the neocortex at either E15 (Figure 1D) or E18 (Figure 1E). However, by P1, *slit2* is weakly expressed in the basal cortical plate (data not shown). By P5, it is present in layer V (Figure 1F), which contains pyramidal neurons that will give rise to the corticospinal and some of the cortico-cortical projections. The strong band of expression at the bottom of Figure 1F is due to previously reported expression in the CA3 field of the hippocampus (Nguyen Ba-Charvet et al., 1999).

slit3, unlike *slit2*, is expressed in the embryonic neocortex, but only transiently. At E15 (Figure 1G), *slit3* is expressed in the cortical plate/marginal zone, in a manner similar to that of *slit1*. However, its expression rapidly disappears, such that *slit3* is not expressed at either E18 (Figure 1H), P1 (data not shown), or P5 (Figure 1I). By P10 *slit3* is expressed at high levels in layers II/III (this is in contrast to *slit1* and *slit2*) and in layer V (Figure 2E). In the adult, *slit3* expression is detected in all layers except layer IV (Figure 2F).

Thus, during the embryonic period when cortical neurons are completing their migration and projection neurons are extending axons toward the intermediate zone, *slit1* and to some extent *slit3* are expressed in the cortical plate. All of the *slit* genes show layer-specific expression patterns during the early postnatal period, which is a period of extensive dendritic growth and branching, as well as terminal branching of afferent axons. Interestingly, all of the *slit*s continue to be expressed in the adult cortex, which suggests that these factors must

regulate cellular events other than those that are developmentally important.

Expression of *robo* Genes in the Developing Cortex

Three mammalian receptors for the Slits have so far been identified, two of which, Robo1 and Robo2, are expressed in distinct patterns in the cortex. The third, Rig-1 (Robo3), is not expressed in the cortex (data not shown). At E15 and E18, *robo1* is expressed throughout the cortical plate at high levels (Figures 1J and 1K). At this age, *robo2* expression is also restricted to the cortical plate (Figure 1M), but at E18 it is expressed throughout the cortical plate and the intermediate zone (Figure 1N), presumably by neurons migrating through this region. At P1, both receptors are expressed similarly in the cortical plate (data not shown), but by P5 *robo1* is expressed in layers II and V (Figure 1L), while *robo2* is expressed in all cortical layers (Figure 1O).

At P10, low levels of *robo1* expression can be detected in layers II and III and higher levels in layers V and VI (Figure 2G). By adulthood, *robo1* expression is restricted to layer V, and to a lesser extent, layer VI (Figure 2H). This transient expansion of expression around P10 suggests that Robo1 might play a role in shaping connectivity in the upper cortical layers, because this is an important period for activity-dependent plasticity. In contrast, the expression of *robo2* is detected in all cortical layers (with slightly lower levels in layer IV) at P10 (Figure 2I). The main change in *robo2* expression between P10 and adult is a decline in expression in the superficial layers (Figure 2J).

The complex and dynamic expression patterns of the *slit* and *robo* gene expression suggests that different receptor-ligand interactions may regulate a number of different cellular events during cortical development. During the late embryonic and early postnatal period, only *slit1* is expressed in the cortical plate, suggesting that Slit1 may play an important regulatory role in axonal and dendritic development. Therefore, in the remainder of the study, we focused on a functional analysis of Slit1 in cortical development.

Processing of Slit1

Since many of our experiments involved the use of recombinant Slit1 myc-tagged at the C terminus (mSlit1-myc) and expressed in 293T cells, we characterized the forms of Slit1 that were produced by transient transfection in these cells. Conditioned supernatant and a salt wash of the Slit1-expressing cells (to remove membrane-associated proteins) were harvested, dialyzed, and concentrated. When this Slit1 supernatant was subjected to SDS-PAGE and Western blotted with α-myc, a band corresponding to full-length Slit1 was detected at the expected molecular weight of $\sim$200 kDa in both the conditioned media and the membrane-associated fraction (Figure 3A). A smaller species of $\sim$40 kDa, corresponding to a smaller C-terminal myc-tagged fragment, was detected in the conditioned media, suggesting that Slit1 undergoes proteolytic processing. This aspect of Slit1 processing is similar to that of Slit2, which is cleaved between the fifth and sixth EGF repeats, resulting in a larger N-terminal fragment of $\sim$140 kDa and a smaller C-terminal fragment of $\sim$55–60 kDa (Brose et al., 1999). The difference in cleavage patterns and product size, coupled with the previously reported divergence in the putative cleavage consensus sequence (Brose et al., 1999), suggests that Slit1 might be cleaved at a different site than Slit2.

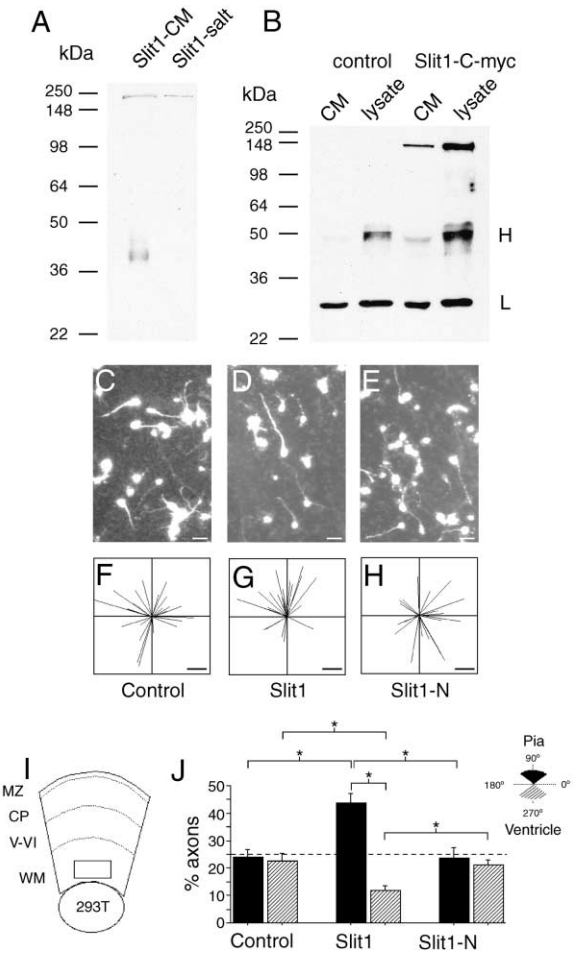

Figure 3. Processing of Slit1 and Effects of Slit1 on Cortical Axon Guidance

(A) Western blot of C-terminal myc-tagged Slit1 found in either the conditioned media (CM) or the salt wash of transiently transfected 293T cells.

(B) Western blot of myc-tagged Slit1 immunoprecipitated from transfected primary cortical neurons. "H" indicates heavy chain, and "L" indicates light chain.

(C–E) Representative images of axon outgrowth, and (F–H) vector diagrams of the axons after 4–6 hr for a 293T aggregate transfected with (C and F) control plasmid, (D and G) full-length Slit1, or (E and H) N-terminal truncated Slit1 (Slit1-N). The scale bars equal 25 μm in (C–H).

(I) Schematic of slice overlay assay in which a transfected 293T aggregate was placed against the white matter of a cortical slice and DiI-labeled cells were plated on top.

(J) Quantification of direction of axon outgrowth in response to transfected 293T aggregate. Asterisks indicate $p < 0.05$ (Student's t test).

To determine if Slit1 is similarly processed in neurons, rat E18 primary neuron cultures were transfected at 3 days in vitro (DIV) with either control or mSlit1-myc plasmid. After 5 DIV, Slit1 from the conditioned media and cell lysates was immunoprecipitated by incubation with

α-myc antibodies. SDS-PAGE followed by blotting with α-myc detected full-length Slit1 which migrates at ~200 kDa (Figure 3B). The cleaved form of Slit1 was not detected in these neuronal transfections, although the possibility that that is due to limits of sensitivity cannot be excluded.

Slit1 Functions as a Chemorepellant for Cortical Axons

In the first series of experiments, we examined the effects of Slit1 on cortical axon guidance using a slice overlay assay (Polleux et al., 1998). Briefly, P2–P3 rat brains were sliced at 250 μM, pieces of neocortex including the cortical plate and the white matter were microdissected, and these cortical slices were cultured on a membrane at an air-media interface. Dissociated rat E18 neurons were labeled with DiI and plated on top of the cortical slices. These neurons adhered to the cortical slice and extended axons within a few hours. Images of the slice with the DiI-labeled neurons were captured with a digital camera, and vectors corresponding to the direction of axon outgrowth recorded.

As previously described (Polleux et al., 1998), a large fraction of the cells landing on the cortical plate extend axons directed toward the white matter. However, those cells landing on the white matter orient their axons randomly. To determine if axon orientation could be influenced by secreted Slit1, we transfected 293T cells with a control vector or with a plasmid expressing mSlit1-myc and placed aggregates of the cells next to the white matter in a slice overlay assay (Figure 3I).

When 293T cells transfected with a control vector were placed next to the white matter, the cortical axons in the adjacent white matter were oriented randomly. Of the axons, 24.1% ± 2.7% were directed toward the pia, and 22.4% ± 2.7% were toward the white matter (Figures 3C, 3F, and 3J). In contrast, when mSlit1-myc was transfected into the 293T cells, 43.6% ± 3.6% of the axons grew away from the aggregate, while only 11.8% ± 1.7% grew toward it, indicating that Slit1 is repellant for cortical axons (Figures 3D, 3G, and 3J). The repulsive effect of Slit1 is quite robust at a distance; the repellent activity could reliably be detected between 250 and 500 μm away from the aggregate-white matter interface, suggesting that a gradient of Slit1 in the cortical plate might contribute to directing newly extending axons toward the white matter.

Slit1 Induces Dendritic Growth and Branching in Cortical Cultures

To determine whether Slit1 might have effects on neuronal morphology apart from its ability to repel axons, we needed to develop a cell culture system that would allow us to analyze the dendritic morphology of individual neurons in culture. To do this, we took advantage of mice that express green fluorescent protein (GFP) in all tissues (Okabe et al., 1997). Male mice heterozygous for the GFP transgene were mated to wild-type females, and the embryos were harvested at E15. The cortices from GFP-expressing and wild-type embryos were dissociated separately, and GFP-positive neurons were diluted at 1:200 with neurons from wild-type littermates and cultured on glass coverslips. Because of this dilution, individual GFP-positive cells in these cultures are well separated from each other, allowing their morphology to be clearly visualized (e.g., Figures 4A–4F). To evaluate the effects of Slit1 on neuronal morphology, supernatant from control and Slit1-transfected 293T cells was concentrated and added to these cultures 1 hr after plating. The cultures were fixed after 3 DIV and stained with α-GFP and α-MAP2, and their morphology was examined under immunofluorescence.

Remarkably, we discovered a robust effect of Slit1 on the growth and branching of cortical neuron dendrites. As shown in Figures 4A–4H, Slit1-treated neurons had visibly more complex dendritic morphologies than controls. To quantify the effects of Slit1 on dendritic branching, GFP-positive neurons from control and Slit1-treated cultures were captured with a digital video camera (Figures 4A–4F), and their dendritic trees were reconstructed and quantified for total dendritic length, number of primary or basal dendrites per cell, and the number of branchpoints per cell. Representative reconstructed cells are shown in Figures 4G and 4H. Cells were also classified as pyramidal or nonpyramidal on the basis of morphological features to determine if Slit1 had different effects on subpopulations of cells. Results remained consistent and statistically significant even if neurons were not grouped by morphology, indicating that our grouping criteria did not introduce bias into the analysis (data not shown). For this and all subsequent dendrite analysis, experiments were repeated at least twice and the results pooled.

We found, in the case of nonpyramidal cells, that Slit1 supernatant caused an increase in the total dendritic length, from 331 ± 28 μM to 423 ± 28 μM (Figure 4I), no statistically significant change in the number of primary dendrites per cell (Figure 4J), and an increase in the average number of branchpoints per cell, from 10.6 ± 1.0 to 17.2 ± 1.2 (Figure 4K). For pyramidal cells, the total dendritic length increased from 286 ± 22 μM to 466 ± 45 μM (Figure 4I), the number of basal dendrites increased from 2.5 ± 0.3 to 3.5 ± 0.3 (Figure 4J), and the number of branchpoints per cell increased from 7.7 ± 0.8 to 14.5 ± 1.7 (Figure 4K) in the presence of Slit1 supernatant. To control for the possibility that the increase in branchpoints may be secondary to overall dendritic arbor expansion rather than a specific effect on branching, we normalized these parameters into a branching index, a measure of the number of branchpoints per average dendritic length. With control-treated cells normalized to 100, we see a 60% increase in the branching index for nonpyramidal cells and a 47% increase for pyramidal cells (Figure 4L). Slit1-induced branches appeared to be evenly distributed, rather than being concentrated at proximal or distal sites. Slit1 treatment also appeared to be correlated with an increase in the number of filopodial-like ruffles on dendritic branches (data not shown). Thus, Slit1 acts as a dendritic branching factor both for pyramidal and nonpyramidal neurons in culture.

Differing Effects of Slit1 and Slit1-N

As previously described, transfection of full-length Slit1 in 293T cells leads to the production of full-length Slit1 and a cleaved fragment. To determine if the full-length

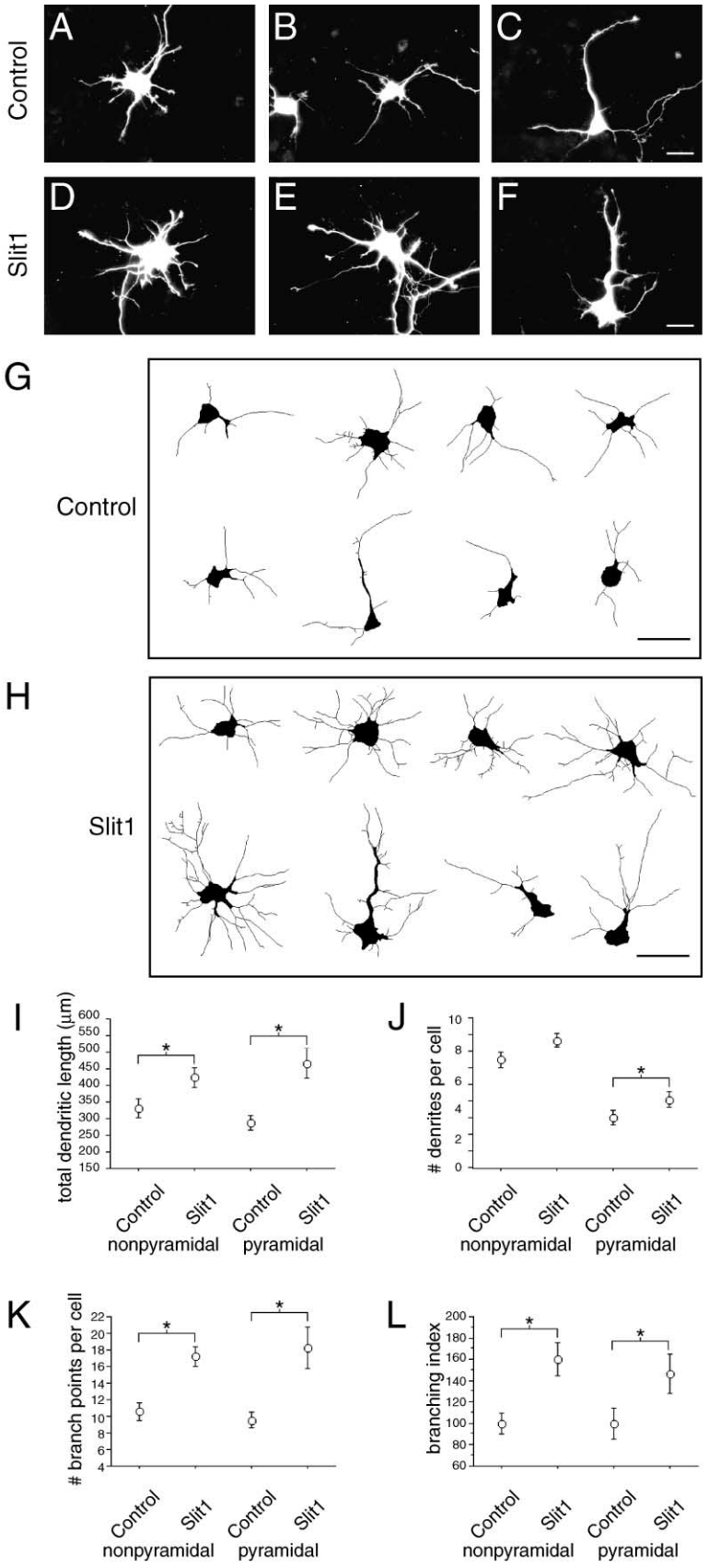

Figure 4. Effects of Slit1 on Dendritic Growth and Branching

(A–F) Examples of GFP+ neurons in GFP:wt mouse cultures treated with either control (A–C) or Slit1 (D–F) supernatant for 3 DIV and stained for α-GFP.

(G and H) Video camera lucida drawings of the dendritic trees of (G) control or (H) Slit1-treated cells. The dendrites of GFP+ neurons were captured, reconstructed, identified as pyramidal or nonpyramidal based on morphological criteria, and quantified with respect to (I) total dendritic length, (J) the number of primary dendrites per nonpyramidal cell or the number of basal dendrites per pyramidal cell, (K) the number of branchpoints per cell, and (L) the branching index, a measure of the number of branchpoints per average dendritic length, normalized to control. The scale bars equal 40 μM in (G) and (H). Asterisks indicate $p < 0.05$ (Student's t test).

and cleaved forms have distinct effects with respect to axonal and dendritic patterning, we constructed an N-terminal Slit1 (Slit1-N) that is truncated between the fifth and sixth EGF repeats, based on the site of cleavage of Slit2. When supernatant was prepared with this construct and added to cultures, it caused a 35% increase in the branching index (data not shown), indicating that the N-terminal fragment retains at least some of the dendritic branching activity. However, when this N-terminal construct was transfected into 293T cells and used in the slice overlay assay, we failed to detect any repellant activity (Figures 3E, 3H, and 3J). This experiment suggests the possibility that full-length and N-terminal Slit1 may differentially influence axon guidance and dendritic branching, but we should emphasize that rigorous evaluation of that possibility will require mapping of the cleavage site for Slit1, which has not yet been done.

Inhibition of Dendritic Branching by Robo Ectodomains

Since the effects of Slit1 on dendrite branching are distinct from previously described biological activities of Slits, in the remainder of the study we focused on characterizing this effect in greater detail. To explore the possibility that endogenous Slits in the primary neuronal cultures might contribute to dendritic branching, we purified Robo ectodomains (the extracellular portion of the Robo1 or Robo2 receptor fused to an Fc domain, Robo1-Fc and Robo2-Fc) and added them to our mouse E15 GFP:wt cultures at 1 μg/ml. Such receptor bodies have previously been used as inhibitors of ligand activity (Cabelli et al., 1997) and would be expected to bind and inhibit extracellular Slits in the cultures (Wu et al., 1999). Consistent with this idea, we found that Robo2-Fc treatment led to a marked decrease in the levels of dendritic growth and branching (Figures 5A and 5B). The total dendritic length of nonpyramidal cells decreased from 520 $\pm$ 50 μM to 255 $\pm$ 25 μM (Figure 5C), the number of primary dendrites decreased from 6.4 $\pm$ 1.7 to 4.2 $\pm$ 1.4 (Figure 5D), and the number of branchpoints decreased from 15.9 $\pm$ 2.4 to 5.5 $\pm$ 0.9 (Figure 5E). Similarly, for pyramidal cells, the total dendritic length decreased from 375 $\pm$ 36 μM to 253 $\pm$ 27 μM (Figure 5C), and the number of branchpoints decreased from 9.9 $\pm$ 1.3 to 6.0 $\pm$ 1.1 (Figure 5E). However, the number of basal dendrites was not affected (Figure 5D).

Both Robo1-Fc and Robo2-Fc were equally effective in reducing branching in these cultures, and this effect could be rescued by preincubating the Robo-Fc protein with Slit1, but not control, supernatant prior to adding it to the cultures (data not shown). In sum, following treatment with Robo-Fc, the branching index decreased by 53% for nonpyramidal cells and 30% for pyramidal cells (Figure 5F), suggesting that endogenous Slits contribute significantly to the branching pattern of cortical neurons in culture.

To determine whether endogenous Slit influences dendritic branching in a more physiological setting, we performed a modified slice overlay assay (Polleux et al., 2000). E17.5 GFP cortical cells were plated on top of P2 rat slices, an age at which Slit1 is still expressed at high levels through most of the cortical plate. Slices were fixed after 7 DIV of incubation with or without 1.5 μg/ml Robo1-Fc and stained for α-GFP and α-MAP2. As in vivo, the apical dendrites of these neurons develop earlier than the basal dendrites, so our analysis was restricted to measurements of apical dendrite length and branching. As shown in Figure 6, Robo-Fc treatment led to marked attenuation of apical dendrite growth and branching. Control cells had an average of 271 $\pm$ 20 μm of total apical dendrite length, compared to 182 $\pm$ 14 μm for Robo1-Fc-treated cells (Figure 6G). The number of branchpoints per apical dendrite in Robo-Fc-treated slices dropped by a factor of 3 (Figure 6H), and the branching index dropped by about 50% (Figure 6I). These observations suggest that endogenous Slit produced by cortical slices acts as a dendritic branching factor and supports the conclusions of the dissociated culture experiments.

Dominant-Negative Robo Constructs Inhibit Dendritic Branching

While the experiments described above suggest that Slits function as dendritic growth and branching factors, they do not address whether Robo receptors mediate this effect. Previous studies indicate that the Robo receptors can multimerize (Simpson et al., 2000b) and that constructs including the extracellular and transmembrane domains but lacking the cytoplasmic domains (designated Robo1-Δ-cyt and Robo2-Δ-cyt, Figure 7A) act as dominant negatives (Stein and Tessier-Lavigne, 2001). Genetic evidence from *Drosophila* also suggests that Robo lacking the cytoplasmic domain might act as a dominant-negative receptor (Bashaw et al., 2000).

To determine whether signaling via Robo receptors was required for Slit-induced dendritic branching, we transfected rat E18 primary rat cortical cultures at 3 DIV with eGFP and either parent vector, Robo1-Δ-cyt or Robo2-Δ-cyt. After 6 DIV the cultures were fixed, and the dendritic morphology of transfected neurons was analyzed following α-GFP and α-MAP2 immunofluorescence. Because the previously described Slit1 effects were not substantially different between nonpyramidal and pyramidal cells, we did not divide our analysis based on cell subtype. As shown in Figure 7, transfection with dominant-negative Robo constructs significantly attenuated Slit-induced dendritic growth and branching. Dendritic length in controls was 333 $\pm$ 23 μM compared to 263 $\pm$ 23 μM for Robo1-Δ-cyt but was essentially unchanged (314 $\pm$ 27 μM) for Robo2-Δ-cyt (Figure 7B). In the control condition, the mean number of dendrites per cell was 4.9 $\pm$ 0.5, which decreased to 3.0 $\pm$ 0.3 and 3.5 $\pm$ 0.3 for Robo1-Δ-cyt and Robo2-Δ-cyt, respectively (Figure 7C). The mean number of branchpoints per cell in controls was 9.0 $\pm$ 1.2 but decreased to 3.2 $\pm$ 0.5 for Robo1-Δ-cyt and to 5.7 $\pm$ 0.8 for Robo2-Δ-cyt (Figure 7D). Overall, Robo1-Δ-cyt was more effective at inhibiting branching, causing a $\sim$70% reduction in the branching index, versus $\sim$50% reduction for Robo2-Δ-cyt (Figure 7E).

To further investigate the role of Robo signaling in the regulation of dendritic branching, we examined whether perturbing Robo signaling in slice cultures would affect dendritic morphology. P8 is the earliest age at which we can reliably use biolistic transfection to introduce

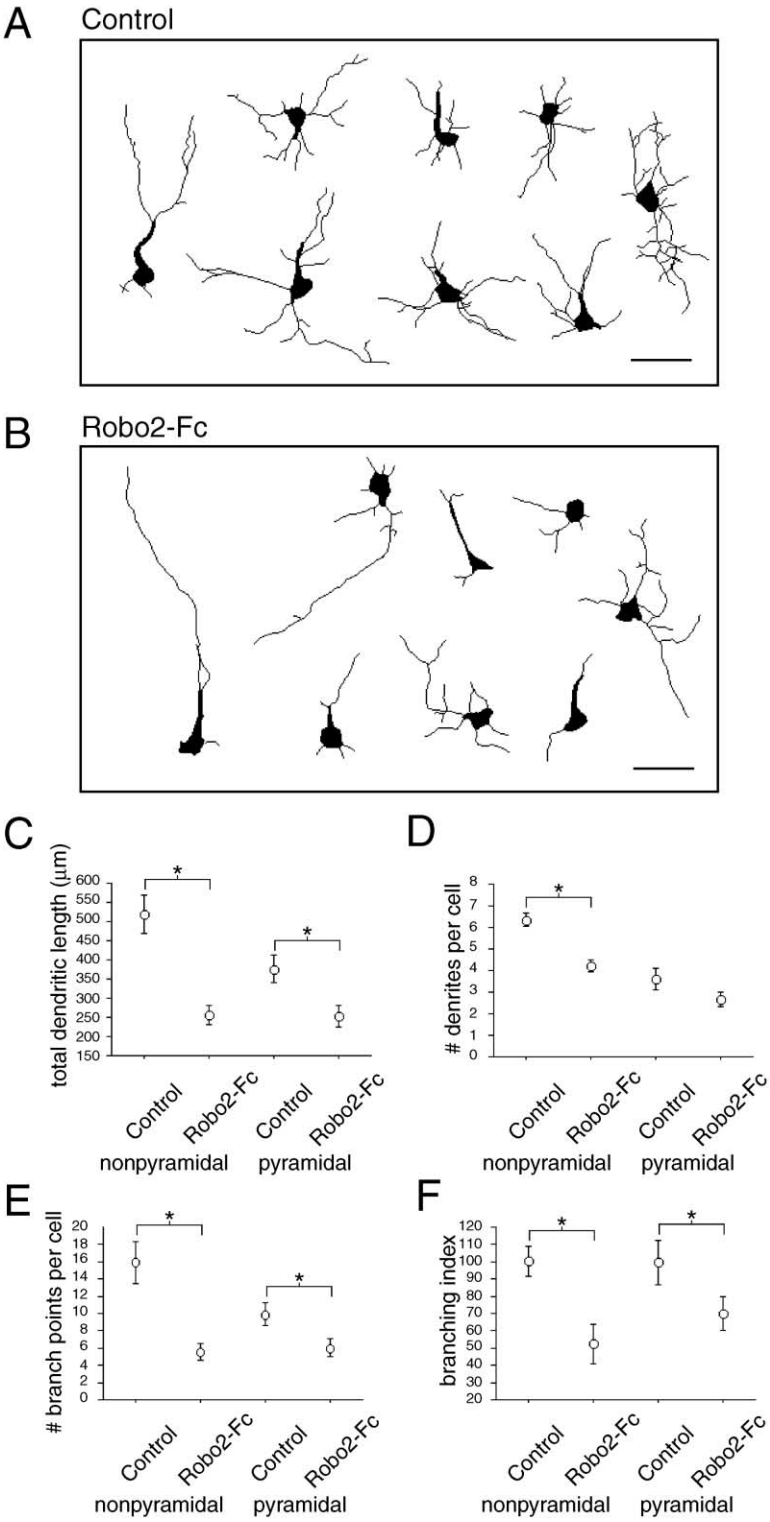

Figure 5. Incubation with Robo-Fc Soluble Extracellular Domain Inhibits Dendritic Branching in Primary Cortical Cultures

(A and B) Video camera lucida drawings of the dendritic trees of E15 mouse cortical neurons treated with either (A) control protein or (B) 1 μg/ml Robo2-Fc for 3 DIV and quantified with respect to (C) total dendritic length, (D) the number of primary dendrites per nonpyramidal cell or the number of basal dendrites per pyramidal cell, (E) the number of branchpoints per cell, and (F) the branching index. The scale bars equal 40 μM in (A) and (B). Asterisks indicate $p < 0.05$ (Student's t test).

constructs into a large number of pyramidal neurons in cortical slices. At this age, layer V pyramidal neurons express both Robo1 and Robo2 mRNA, suggesting that they may be responsive to any or all of the Slits expressed in the cortex. Cortical slices (400 μm) were cultured for 1 DIV before being transfected with control plasmid plus eGFP (Figures 7F–7H) or Robo1-Δ-cyt plus eGFP (Figures 7I–7K) and fixed at 3 DIV. Slices were stained with α-GFP and α-MAP2, and the nuclei were counterstained with Hoescht dye to assist with the assignment of laminar identity. Transfected layer V pyramidal neurons were captured with a confocal microscope. Merged Z stack images were subjected to a modified Sholl analysis, in which a series of concentric rings are

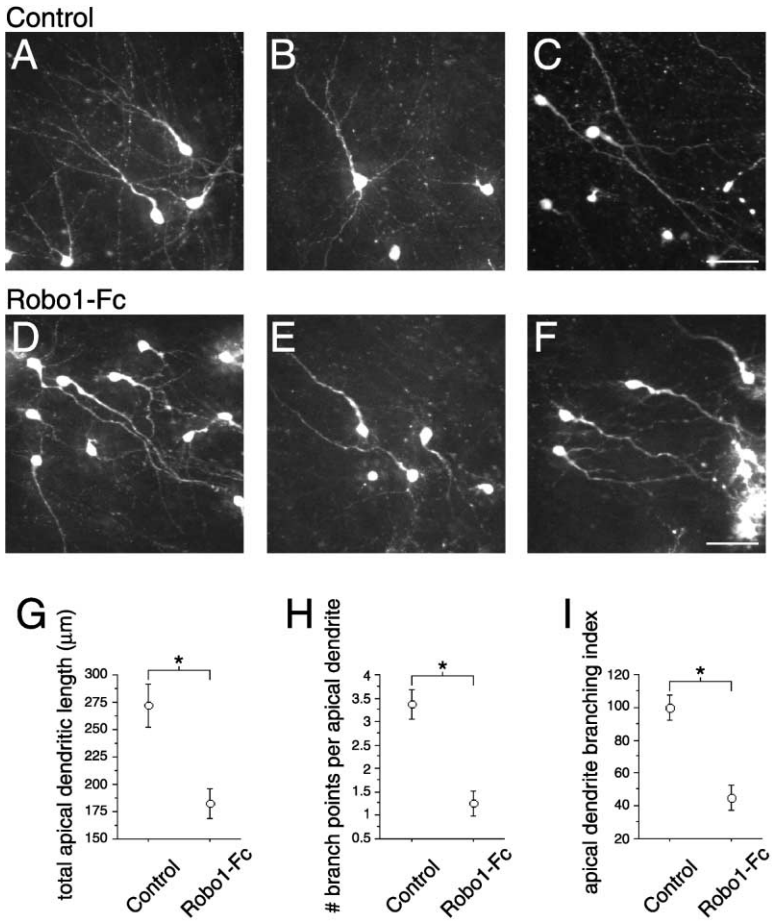

Figure 6. Incubation with Robo-Fc Soluble Extracellular Domain Inhibits Dendritic Branching in a Modified Slice Overlay Assay

(A–F) Merged confocal images of control-treated (A–C) or Robo1-Fc-treated (D–F) GFP+ neurons from slice overlay cultures in which E17.5 GFP mouse cells were plated onto P2 rat slices and cultured for 7 DIV with control (Alkaline Phosphatase-Fc) or Robo1-Fc protein.

Neurons with an apical dendrite were quantified with respect to (G) total apical dendritic length, (H) the number of branchpoints per apical dendrite, and (I) the branching index for apical dendrites. The scale bars equal 50 μm. Asterisks indicate $p < 0.05$ (Student's t test).

centered on the cell body and the number of processes crossing each of the rings is counted. This analysis indirectly measures both dendritic length and branching, giving rise to a measure of dendritic complexity.

Robo1-Δ-cyt-transfected neurons appeared to have both fewer and shorter dendritic processes (Figures 7I–7K) than did control-transfected cells (Figures 7F–7H). Quantitative analysis revealed that apical dendrites showed a statistically significant reduction in dendritic complexity as measured by the Sholl analysis at all points between 25 and 250 μm from the cell body, with one exception (Figure 7L). Basal dendrites showed a similar reduction between 25 and 75 μm away from the cell body (Figure 7M). This experiment indicates that inhibition of Robo signaling is sufficient to attenuate dendritic branching in layer V pyramidal neurons.

Met-Robo Chimeric Receptors Induce Dendritic Branching in Response to HGF Stimulation

In order to determine whether activation of Robo receptors is sufficient to induce dendritic branching, we utilized Met-Robo chimeric receptors. In these constructs, the extracellular domain of Met, the hepatocyte growth factor (HGF) receptor, is fused to the transmembrane and cytoplasmic domains of Robo1 or Robo2. Addition of HGF causes dimerization of the Met domains and activation of Robo signaling (Stein and Tessier-Lavigne, 2001). When 100 ng/ml HGF was added to E18 rat cultures cotransfected with eGFP and control vector, there was no effect on any of the dendritic parameters measured previously (data not shown). However, transfection of Met-Robo1 or Met-Robo2 followed by HGF stimulation led to a dramatic increase in both dendritic growth and branching (Figures 8A and 8B). For Met-Robo1, total dendritic length increased from 397 ± 21 μM to 523 ± 36 μM (Figure 8E), the number of dendrites per cell increased from 3.2 ± 0.2 to 4.0 ± 0.2 (Figure 8F), and the number of branchpoints per cell increased from 4.7 ± 0.4 to 10.0 ± 1.1 (Figure 8G). Met-Robo2 behaved in a very similar manner; total dendritic length increased from 388 ± 25 μM to 479 ± 21 μM (Figure 8E), the number of dendrites per cell increased from 3.4 ± 0.2 to 4.2 ± 0.3 (Figure 8F), and the number of branchpoints increased from 5.3 ± 0.5 to 9.9 ± 0.6 (Figure 8G). Strikingly, upon stimulation with HGF, the branching index for cells transfected with either Met-Robo1 or Met-Robo2 doubles (Figure 8H), indicating that activation of the intracellular domain of either Robo1 or Robo2 is sufficient to reproduce the dendritic growth and branching induced by stimulation with Slit1.

Discussion

Our experiments indicate that Slit-Robo interactions can exert considerable influence on the development of axons and dendrites in cortical neurons. In a slice overlay

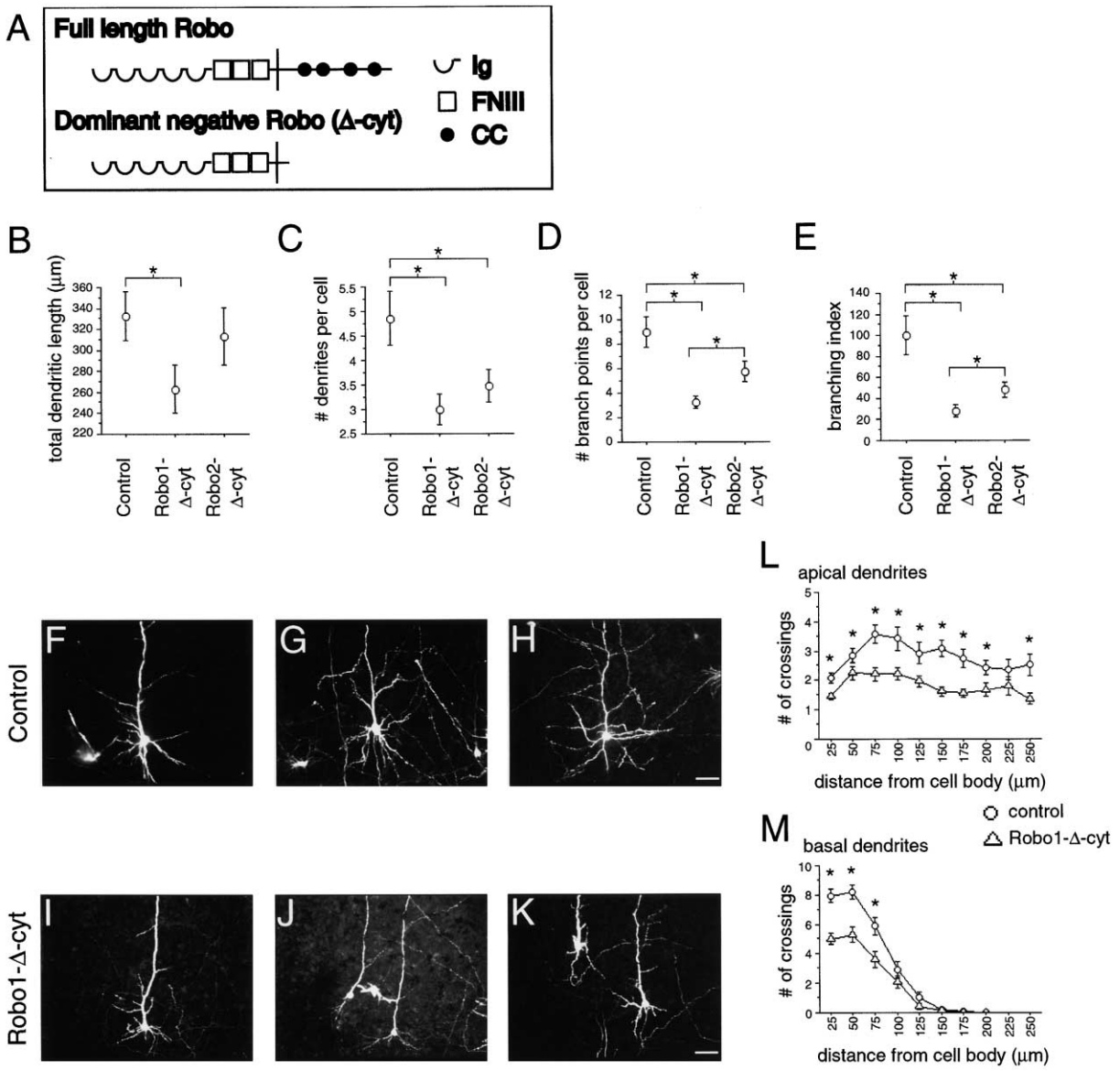

Figure 7. Transfection of Dominant-Negative Robo Inhibits Dendritic Branching

(A) Schematic of dominant-negative Robo receptor constructs with a cytoplasmic deletion. Abbreviations are as follows: Ig, immunoglobulin domain; FNIII, fibronectin type three repeat; and CC, conserved cytoplasmic motif.

(B–E) Control plasmid, Robo1-Δ-cyt, or Robo2-Δ-cyt were transfected, along with eGFP plasmid, into rat E18 primary neuron cultures at 3 DIV and fixed at 6 DIV. GFP+ neurons were scored for (B) total dendritic length, (C) the number of dendrites per cell, and (D) the number of branchpoints per cell, and these parameters were normalized as (E) the branching index.

(F–K) Merged confocal images of layer V pyramidal neurons from P8 rat slices biolistically transfected with eGFP and control plasmid (F–H) or Robo1-Δ-cyt (I–K). The scale bars equal 50 μm.

(L and M) Modified Sholl analysis reflecting dendritic complexity for (L) apical dendrites or (M) basal dendrites. Asterisks indicate $p < 0.05$ (Student's t test).

assay, Slit1 is a chemorepellant for cortical axons, and the developmental expression of Slit1 suggests that it may orient axons toward the white matter. Along with repelling axons, we find that Slit1 has a striking and robust effect on dendritic growth and branching. We find that addition of Robo-Fc, which should bind and inhibit extracellular Slit, inhibits dendritic growth and branching both in dissociated cultures and in slice overlay assays. We also find that expression of a dominant-negative Robo construct attenuates dendritic branching in dissociated cultures and in cortical slice cultures, suggesting that endogenous Slit acts as a branching factor for cortical neurons. Activation of the Robo receptor appears to be sufficient to induce dendritic growth and branching, since these effects can be induced by HGF stimulation of neurons expressing a Met-Robo chimeric receptor. These observations reveal a new role for Slits in the control of dendritic development, and suggest that Slit1 in particular may play a critical role in specifying cortical neuron morphology. The effects

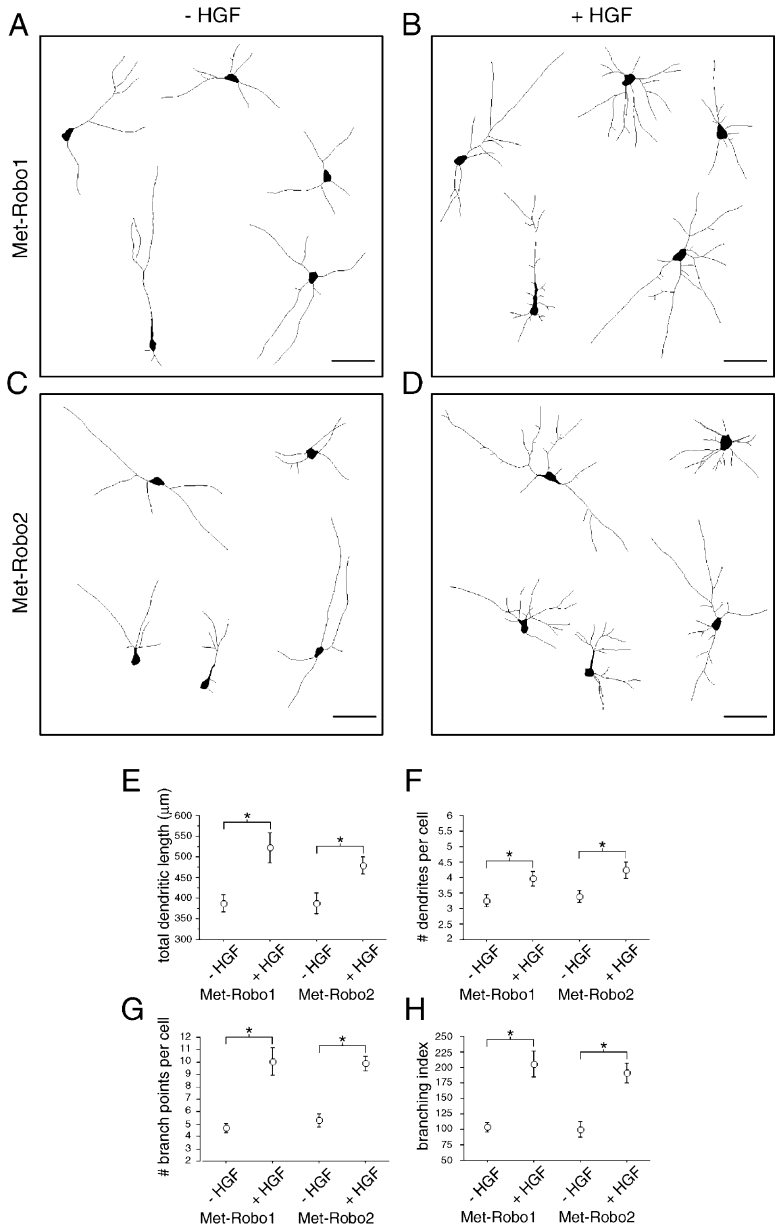

Figure 8. HGF Stimulation of Neurons Expressing Met-Robo Chimeric Receptors Induces Dendritic Branching

Rat E18 cortical neurons were transfected with Met-Robo1 or Met-Robo2 at 3 DIV, stimulated at 4 DIV with 100 ng/ml hepatocyte growth factor (HGF), and fixed at 7 DIV. Representative reconstructed neurons transfected with (A) Met-Robo1 without HGF stimulation, (B) Met-Robo1 with 100 ng/ml HGF, (C) Met-Robo2 without HGF, or (D) Met-Robo2 stimulated with 100 ng/ml HGF. Quantification of transfected and unstimulated versus stimulated cells for (E) total dendritic length, (F) the number of dendrites per cell, (G) the number of branchpoints per cell, and (H) the branching index. The scale bars equal 50 μM in (A–D). Asterisks indicate $p < 0.05$ (Student's t test).

of Slit1 on dendritic branching are similar to the effect of the N-terminal fragment of Slit2 on dorsal root ganglion axons (Nguyen Ba-Charvet et al., 2001; Wang et al., 1999), and together these studies suggest that regulation of branch formation may be a general property of Slit proteins.

It is interesting to consider the effects of Slit1 in the context of its developmental expression. We detect Slit1 expression in the cortical plate as early as E15. At this time only layer 5 and 6 cells have migrated into the cortical plate and have just extended an efferent axon toward the intermediate zone. Based on the ability of Slit1 to repel cortical axons, we propose that this early expression of Slit1 is involved in axon repulsion. One would expect a gradient of Slit1 to be present in the cortical plate at this age, but unfortunately in the absence of an antibody to Slit1, we cannot make definitive conclusions about the distribution of the protein. This has been a general problem with all of the secreted guidance cues, and in the future it will be important to develop tools to visualize these proposed gradients to place guidance models on firmer footing.

We initially began studying the Slit family of secreted chemorepellants in search of a Sema3A-independent activity in the cortical plate that contributed to the proper orientation of cortical axons toward the white matter. Slit1, like Sema3A, is highly expressed in the cortical plate during the period when axons are initially projecting to the white matter, and like Sema3A, Slit1 is capable of repelling cortical axons in a slice overlay assay. The functional significance of having two chemorepellants similarly expressed in the cortical plate is not clear, but one possibility is that they act on different subsets of cortical projection neurons. Interestingly,

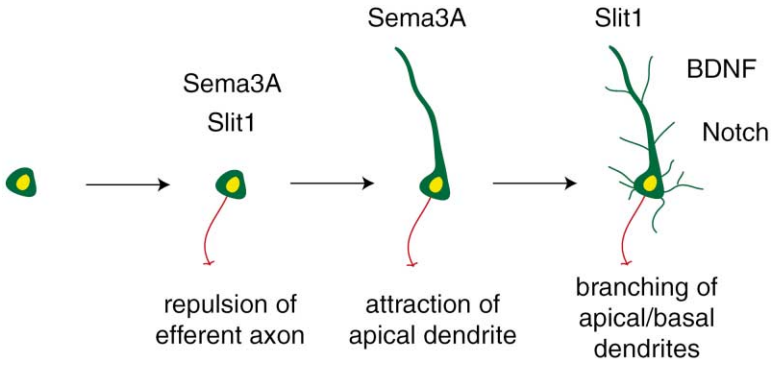

Figure 9. A Model of How Sequential Action of Extracellular Factors Might Specify Cortical Neuron Morphology

A newly postmitotic neuron arrives at the cortical plate, where it encounters gradients of Sema3A and Slit1, thereby directing its initial axon trajectory toward the white matter. The same gradient of Sema3A attracts the apical dendrite of the neuron toward the pial surface. Other factors such as BDNF, Notch, and Slit1 control the growth and branching of dendrites.

Slit2 can also function as a chemorepellant for cortical axons (K.L.W., A.G., unpublished data). Based on reports of Slit2 expression in the ventral diencephalon (Ringstedt et al., 2000), it seems that Slit2 may guide cortical efferents to the thalamus. Additionally, Slit2 expressed at the midline may control the crossing of callosal fibers (Shu and Richards, 2001). If this is the case, the set of Slit family members may serve to direct cortical axons at multiple points in their trajectories.

From E18 to P10, the expression of Slit1 is most prominent in the deep cortical layers and the subplate. This period is characterized by elaboration and branching of basal dendrites and apical dendrite collateral formation in layer V/VI neurons. Based on the expression pattern and cellular effects of Slit1, we believe that this late embryonic and early postnatal expression is mainly involved in regulating dendritic growth and branching in deep-layer cortical neurons. Dendritic branching in superficial-layer neurons might be regulated by Slit1 that diffuses to those layers, or it could be regulated by other factors such as neurotrophins, which have also been shown to affect cortical dendrite branching and are expressed in superficial cortical layers (McAllister et al., 1995, 1997).

It is interesting to note that all three Slits have layer-restricted expression during postnatal development and in adulthood. The layer-specific expression during early postnatal development may be important in regulating layer-specific apical dendrite collateral branching or layer-specific axon terminations. For example, *slit3* is expressed at high levels in most layers at P10 except layers IV and VI, which are the recipient layers for thalamic axons. It will be interesting to know whether a repulsive effect of Slit3 prevents innervation of layers II/III and V by these axons. It is also striking that all three *slits* as well as *robos* are expressed at high levels in the adult cortex, which suggests that Slit-Robo interactions must influence cellular events other than axon guidance and dendritic patterning. Although not much is known about how Slits are secreted, based on the in situ hybridization studies and the results of Robo-Fc blocking experiments in essentially pure neuronal cultures, it would appear that Slit proteins are secreted by neurons.

How is the Slit signal transduced to mediate changes in axonal and dendritic morphology? The dominant-negative Robo and Met-Robo transfection experiments suggest that the signal is transduced via the Robo receptor(s). Relatively little is known about mechanisms of Robo signaling, but activation by Slit binding must ultimately lead to changes in the cytoskeleton to be able to modify the axon growth cone or dendritic dynamics. The VASP family member Enabled (Ena), which plays a role in regulating the actin cytoskeleton, binds the intracellular polyproline-rich CC2 motif in Robo and contributes to its repulsive output (Bashaw et al., 2000). Mutations in Ena can also perturb the formation of dendrites, and therefore Ena may play a role in mediating Slit1 effects on dendritic branching (Gao et al., 1999). The Rho family of GTPases may also participate in the dendritic branching response to Slit, perhaps by increasing branch dynamics or stabilizing branches. Rac and Cdc42, members of this family, have previously been shown to play such a role for dendrites (Li et al., 2000; Threadgill et al., 1997). It will be of interest to determine if Robo recruits activators or effectors of these GTPases to the membrane as a means of regulating cytoskeletal change (Bokoch et al., 1996; Galisteo et al., 1996). The ability of the Met-Robo chimeric receptors to induce branching upon stimulation with HGF should provide a useful assay for identifying regions of the receptor that are required for this response.

The experiments described here add to recent advances in identification of signals that regulate axonal and dendritic development in cortical neurons. These observations suggest a model (Figure 9) in which neurons arriving at the cortical plate encounter gradients of both Sema3A and Slit1, which repel the newly formed efferent axons toward the white matter. The same source of Sema3A also functions as a chemoattractant for apical dendrites and specifies the axis of polarity of the neuron. The elaboration of primary dendrites may then be initiated in response to extracellular BDNF (McAllister et al., 1995, 1997), and the elongation of dendritic processes may be regulated both by BDNF and Slit1. Finally, signaling by Slit1 and Notch appear to regulate dendritic branching and the extent of dendritic growth (Redmond et al., 2000). Thus, the sequential influence of several extracellular signals specifies the final morphology of cortical neurons, which in turn has a critical effect on neuronal connectivity.

Experimental Procedures

In Situ Hybridization

All cDNAs encoding rat Slit1, Slit2, Robo1, and Robo2 were subcloned in pBluescript. The probes for rSlit1 and rSlit2 correspond to 800 bp and 1600 bp fragments, respectively, as previously reported (Brose et al., 1999). rSlit3 was subcloned in pCR-II-topo and corresponded to a 1749 bp fragment encoding a portion of the LRR4

motif and the beginning of the EGF motifs, before the cleavage site. rRobo1 cDNA corresponds to a 1000 bp fragment spanning the first three immunoglobulin motifs, while the rRobo2 cDNA was a 1000 bp fragment encoding the end of the third immunoglobulin motif. Probes were made using the Promega kit and labeled with digoxigenin-11-dUTP.

Plasmids

The mSlit1-myc (Wu et al., 1999), Robo1-Δ-cyt, Robo2-Δ-cyt, Met-Robo1, and Met-Robo2 (Stein and Tessier-Lavigne, 2001) plasmids used in this study have been previously described. Slit1-N contains the coding sequence for human Slit1 through the fifth EGF repeat. Robo1-Fc and Robo2-Fc were created by fusing the extracellular domain of Robo1 and Robo2, respectively, to the immunoglobulin Fc domain.

Slit1 Supernatant and Robo-Fc Preparation

Dishes (70% confluent; 10 cm) of 293T cells were Lipofectamine (GIBCO-BRL) transfected with 10 μg mSlit1-myc or parent pCS2 vector. The following day, media was changed to Optimem or DMEM plus 10% FBS and harvested at 3 DIV. Cells were washed with 1M NaCl and 10 mM HEPES (pH 7.4). For Western analysis, the salt fraction was dialyzed and both were concentrated (Amicon Centriprep). For supernatant preparation, the fractions were pooled, dialyzed against phosphate-buffered saline (PBS), concentrated, and 10 μl per 1 ml media added. For Robo-Fc purification, 15 cm dishes of 293T cells were transfected with control plasmid, Robo1-Fc, or Robo2-Fc, and Optimem-conditioned media was incubated with Protein A/G beads (Santa Cruz) for washing and eluting.

Immunoprecipitation and Western Blots

Dishes (60 mm) containing 4×10^6 neurons were transfected with 9 μg control plasmid or mSlit1-myc at 3 DIV. At 6 DIV, conditioned media and cell lysate were collected, incubated with the α-myc monoclonal 9E10 (Babco) and then Protein A/G beads before running on a 12% polyacrylamide gel. After transfer, blots were incubated in primary (9E10, 1:1000) in 0.5% milk in 1X TBST. α-mouse-HRP secondary antibody (Amersham) at 1:20,000 was used and visualized with a chemiluminescent substrate (SuperSignal, Pierce). Slit1 supernatant was subjected to the same Western blotting protocol.

Slice Overlay Assay

Postnatal day 2 or 3 (P2-P3) rat brains were dissected in cold Hanks' balanced salt solution (HBSS), embedded in 3% low-melting point agarose in HBSS, and coronally sectioned on a vibratome at 250 μM. Slices were cultured on a transparent porous membrane (1 μM pore size, Becton Dickinson) in a 35 mm well containing media (70% Basal Media Eagle, 25% HBSS, 20 mM glucose, 1 mM glutamine, 1 mM penicillin-streptomycin, 5% horse serum). Aggregates of transfected 293T cells were prepared using a modified hanging-drop method in which cells were resuspended in rat tail collagen, which was allowed to polymerize. E18 dissociated rat neurons were labeled in DiI (1,1′-dioctadecyl-3,3,3′,3′-tetramethyl indocarbocyanine percholate, Molecular Probes) for 10 min before plating on top of slice-aggregate cocultures. The slices were imaged with IPLab Spectrum 3.1.1 (Scanalytics) 4–6 hr after DiI-labeled dissociated neurons were plated on top of the cortical slice-293T aggregate combination. If a cell landed within 250 μM of the interface between the 293T aggregate and the white matter, a vector representing the direction and length of its axon was drawn. Axon vectors between 45° and 135° were considered to be oriented toward the pia, and those between 225° and 315° as oriented toward the ventricle (and the 293T aggregate; see Figure 3). On average, 20 axons per slice with 5–10 slices per condition were imaged per experiment, and experiments were repeated multiple times. Percentages are indicated as the mean ± standard error. Statistically significant differences (Student's t test, $p < 0.05$) are indicated with an asterisk.

Primary Neuron Cultures

E18 cortical cells from Long-Evans rats and E17.5 mouse cells were cultured as previously described (Threadgill et al., 1997). For E15 mouse cultures, enzymatic dissociation was reduced to twenty minutes and cells were plated in Neurobasal medium supplemented with B27. Both rat and mouse cultures were plated at 1×10^6 cells per well in 12 well dishes containing glass coverslips coated with poly-D-lysine and laminin. Calcium-phosphate transfections were performed as previously described (Threadgill et al., 1997). For each well, 3 μg of experimental plasmid was cotransfected with 1 μg of eGFP (Clontech). HGF was obtained from Calbiochem.

Biolistic Transfection

P8 rat slices were sliced to 400 μm on the Vibratome without embedding, quickly microdissected, and plated on a membrane in the presence of slice culture media with 25% horse serum. At 1 DIV, slices were shot at 180 psi using a GeneGun (BioRad) and 1.6 μm bullets containing a 3:1 mixture of experimental plasmid to eGFP (Clontech). Slices were fixed 48 hr after shooting.

Immunofluorescence

Cultures were fixed with 4% paraformaldehyde in phosphate-buffered saline (PBS) with 4% sucrose, washed in PBS, blocked with 3% bovine serum albumin (BSA) and 0.3% Triton X-100 in PBS, and incubated in primary antibody overnight. α-GFP (Molecular Probes) and α-MAP2 (Sigma) were used at 1:3000 and 1:2000, respectively. Oregon Green- (Molecular Probes) and Cy3 (Jackson Immunoresearch)-conjugated secondary antibodies were at 1:600 in blocking solution with 1% normal goat serum. Nuclei were visualized with Hoescht 33258 (Molecular Probes).

Dendritic Analysis

Slit supernatant, Robo-Fc, and transfection experiments were carried out in duplicate wells, and all of the experiments described here were repeated at least twice and the results pooled. GFP+ neurons were randomly captured using a digital camera attached to a Nikon Eclipse TE300 inverted microscope driven by IPLab or OpenLab image-acquisition software. Thirty to forty neurons per morphological class per condition per experiment were reconstructed and scored for number of processes, total dendritic length, dendritic branchpoints, average dendritic length, and branching index (number of branchpoints divided by average dendritic length, expressed as percent of control). Axons were excluded from analysis on the basis of characteristic morphology or MAP2 negativity. For quantification, the image of each analyzed neuron projected on the computer screen was traced with a virtual pen (using the mouse to move the pen). This trace was used by the software program to calculate total length and other parameters. A subset of cells were reconstructed using ClarisDraw software for representative purposes. For the modified slice overlay assay and biolistic transfections, neurons were acquired on an Ultraview confocal. Z stacks were merged in OpenLab and either quantified as above or subjected to a modified Sholl analysis with concentric circles every 25 μm. The biolistic transfection experiment was performed three times, with a total of 30 cells per condition quantified and the results at each interval compared by an unpaired t test. Data are shown as mean ± standard error. Statistically significant differents (Student's t test, $p < 0.05$) are indicated by an asterisk.

It should be noted that the "controls" in the different experiments are different, depending upon the experimental manipulation. In Figure 4, the control treatment is supernatant from 293T cells transfected with the parent vector, concentrated the same way as the Slit1 supernatants. In Figure 5, the control treatment is AP-Fc protein, purified from 293T cell supernatants the same way as Robo-Fc. In Figure 7, the controls represent neurons transfected with a vector plasmid instead of the dominant-negative Robo construct. Also, the neurons in Figures 4 and 5 are from mice, and in Figure 7 the neurons are from rats, and rat and mouse neurons show somewhat different morphologies even in the same media. The variability in the "control" values, therefore, results from the differences in exact experimental treatment and the source of the cells. Within any experimental manipulation, however, the variability between experiments was small.

Acknowledgments

We thank K. Brose and Y. Rao for mammalian Slit and Robo constructs and A. Kolodkin and L. Redmond for comments on the manu-

script. This work was supported by grants from the National Institutes of Health (NS39993; A.G.), the March of Dimes Birth Defects Foundation (A.G.), the Institut de la Santé et de le Recherche Médicale (INSERM) (A.C.), the Ministère de la Recherche et de la Technologie (A.C.), and the Association pour la Recherche sur le Cancer (A.C.). V.M. is a recipient of a Ministère de l'éducation nationale, de la recherche et de la technologie (MENRT) fellowship. M.T.L. and C.S.G. are investigators of the Howard Hughes Medical Institutes.

Received June 19, 2001; revised October 9, 2001.

References

Bashaw, G.J., Kidd, T., Murray, D., Pawson, T., and Goodman, C.S. (2000). Repulsive axon guidance: Abelson and Enabled play opposing roles downstream of the roundabout receptor. Cell *101*, 703–715.

Bokoch, G.M., Wang, Y., Bohl, B.P., Sells, M.A., Quilliam, L.A., and Knaus, U.G. (1996). Interaction of the Nck adapter protein with p21-activated kinase (PAK1). J. Biol. Chem. *271*, 25746–25749.

Brose, K., Bland, K.S., Wang, K.H., Arnott, D., Henzel, W., Goodman, C.S., Tessier-Lavigne, M., and Kidd, T. (1999). Slit proteins bind Robo receptors and have an evolutionarily conserved role in repulsive axon guidance. Cell *96*, 795–806.

Cabelli, R.J., Shelton, D.L., Segal, R.A., and Shatz, C.J. (1997). Blockade of endogenous ligands of trkB inhibits formation of ocular dominance columns. Neuron *19*, 63–76.

Erskine, L., Williams, S.E., Brose, K., Kidd, T., Rachel, R.A., Goodman, C.S., Tessier-Lavigne, M., and Mason, C.A. (2000). Retinal ganglion cell axon guidance in the mouse optic chiasm: expression and function of robos and slits. J. Neurosci. *20*, 4975–4982.

Fricke, C., Lee, J.S., Geiger-Rudolph, S., Bonhoeffer, F., and Chien, C.B. (2001). astray, a zebrafish roundabout homolog required for retinal axon guidance. Science *292*, 507–510.

Galisteo, M.L., Chernoff, J., Su, Y.C., Skolnik, E.Y., and Schlessinger, J. (1996). The adaptor protein Nck links receptor tyrosine kinases with the serine-threonine kinase Pak1. J. Biol. Chem. *271*, 20997–21000.

Gao, F.B., Brenman, J.E., Jan, L.Y., and Jan, Y.N. (1999). Genes regulating dendritic outgrowth, branching, and routing in Drosophila. Genes Dev. *13*, 2549–2561.

Itoh, A., Miyabayashi, T., Ohno, M., and Sakano, S. (1998). Cloning and expressions of three mammalian homologues of Drosophila slit suggest possible roles for Slit in the formation and maintenance of the nervous system. Brain Res. Mol. Brain Res. *62*, 175–186.

Kidd, T., Brose, K., Mitchell, K.J., Fetter, R.D., Tessier-Lavigne, M., Goodman, C.S., and Tear, G. (1998). Roundabout controls axon crossing of the CNS midline and defines a novel subfamily of evolutionarily conserved guidance receptors. Cell *92*, 205–215.

Kidd, T., Bland, K.S., and Goodman, C.S. (1999). Slit is the midline repellent for the robo receptor in Drosophila. Cell *96*, 785–794.

Kramer, S.G., Kidd, T., Simpson, J.H., and Goodman, C.S. (2001). Switching repulsion to attraction: changing responses to slit during transition in mesoderm migration. Science *292*, 737–740.

Li, H.S., Chen, J.H., Wu, W., Fagaly, T., Zhou, L., Yuan, W., Dupuis, S., Jiang, Z.H., Nash, W., Gick, C., et al. (1999). Vertebrate slit, a secreted ligand for the transmembrane protein roundabout, is a repellent for olfactory bulb axons. Cell *96*, 807–818.

Li, Z., Van Aelst, L., and Cline, H.T. (2000). Rho GTPases regulate distinct aspects of dendritic arbor growth in Xenopus central neurons in vivo. Nat. Neurosci. *3*, 217–225.

McAllister, A.K., Lo, D.C., and Katz, L.C. (1995). Neurotrophins regulate dendritic growth in developing visual cortex. Neuron *15*, 791–803.

McAllister, A.K., Katz, L.C., and Lo, D.C. (1997). Opposing roles for endogenous BDNF and NT-3 in regulating cortical dendritic growth. Neuron *18*, 767–778.

Metin, C., Deleglise, D., Serafini, T., Kennedy, T.E., and Tessier-Lavigne, M. (1997). A role for netrin-1 in the guidance of cortical efferents. Development *124*, 5063–5074.

Nguyen Ba-Charvet, K.T., Brose, K., Marillat, V., Kidd, T., Goodman, C.S., Tessier-Lavigne, M., Sotelo, C., and Chedotal, A. (1999). Slit2-mediated chemorepulsion and collapse of developing forebrain axons. Neuron *22*, 463–473.

Nguyen Ba-Charvet, K.T., Brose, K., Ma, L., Wang, K.H., Marillat, V., Sotelo, C., Tessier-Lavigne, M., and Chedotal, A. (2001). Diversity and specificity of actions of Slit2 proteolytic fragments in axon guidance. J. Neurosci. *21*, 4281–4289.

Niclou, S.P., Jia, L., and Raper, J.A. (2000). Slit2 is a repellent for retinal ganglion cell axons. J. Neurosci. *20*, 4962–4974.

Okabe, M., Ikawa, M., Kominami, K., Nakanishi, T., and Nishimune, Y. (1997). 'Green mice' as a source of ubiquitous green cells. FEBS Lett. *5*, 313–319.

Polleux, F., Giger, R.J., Ginty, D.D., Kolodkin, A.L., and Ghosh, A. (1998). Patterning of cortical efferent projections by semaphorin-neuropilin interactions. Science *282*, 1904–1906.

Polleux, F., Morrow, T., and Ghosh, A. (2000). Semaphorin 3A is a chemoattractant for cortical apical dendrites. Nature *404*, 567–573.

Rajagopalan, S., Vivancos, V., Nicolas, E., and Dickson, B.J. (2000). Selecting a longitudinal pathway: Robo receptors specify the lateral position of axons in the Drosophila CNS. Cell *103*, 1033–1045.

Redmond, L., Oh, S.R., Hicks, C., Weinmaster, G., and Ghosh, A. (2000). Nuclear Notch1 signaling and the regulation of dendritic development. Nat. Neurosci. *3*, 30–40.

Richards, L.J., Koester, S.E., Tuttle, R., and O'Leary, D.D. (1997). Directed growth of early cortical axons is influenced by a chemoattractant released from an intermediate target. J. Neurosci. *17*, 2445–2458.

Ringstedt, T., Braisted, J.E., Brose, K., Kidd, T., Goodman, C., Tessier-Lavigne, M., and O'Leary, D.D. (2000). Slit inhibition of retinal axon growth and its role in retinal axon pathfinding and innervation patterns in the diencephalon. J. Neurosci. *20*, 4983–4991.

Rothberg, J.M., and Artavanis-Tsakonas, S. (1992). Modularity of the slit protein. Characterization of a conserved carboxy-terminal sequence in secreted proteins and a motif implicated in extracellular protein interactions. J. Mol. Biol. *227*, 367–370.

Rothberg, J.M., Jacobs, J.R., Goodman, C.S., and Artavanis-Tsakonas, S. (1990). slit: an extracellular protein necessary for development of midline glia and commissural axon pathways contains both EGF and LRR domains. Genes Dev. *4*, 2169–2187.

Serafini, T., Colamarino, S.A., Leonardo, E.D., Wang, H., Beddington, R., Skarnes, W.C., and Tessier-Lavigne, M. (1996). Netrin-1 is required for commissural axon guidance in the developing vertebrate nervous system. Cell *87*, 1001–1014.

Shu, T., and Richards, L.J. (2001). Cortical axon guidance by the glial wedge during the development of the corpus callosum. J. Neurosci. *21*, 2749–2758.

Simpson, J.H., Bland, K.S., Fetter, R.D., and Goodman, C.S. (2000a). Short-range and long-range guidance by Slit and its Robo receptors: a combinatorial code of Robo receptors controls lateral position. Cell *103*, 1019–1032.

Simpson, J.H., Kidd, T., Bland, K.S., and Goodman, C.S. (2000b). Short-range and long-range guidance by slit and its Robo receptors. Robo and Robo2 play distinct roles in midline guidance. Neuron *28*, 753–766.

Stein, E., and Tessier-Lavigne, M. (2001). Hierarchical organization of guidance receptors: silencing of netrin attraction by slit through a Robo/DCC receptor complex. Science *291*, 1928–1938.

Threadgill, R., Bobb, K., and Ghosh, A. (1997). Regulation of dendritic growth and remodeling by Rho, Rac, and Cdc42. Neuron *19*, 625–634.

Wang, K.H., Brose, K., Arnott, D., Kidd, T., Goodman, C.S., Henzel, W., and Tessier-Lavigne, M. (1999). Biochemical purification of a mammalian slit protein as a positive regulator of sensory axon elongation and branching. Cell *96*, 771–784.

Wu, W., Wong, K., Chen, J., Jiang, Z., Dupuis, S., Wu, J.Y., and Rao, Y. (1999). Directional guidance of neuronal migration in the olfactory system by the protein Slit. Nature *400*, 331–336.

Yuan, S.S., Cox, L.A., Dasika, G.K., and Lee, E.Y. (1999). Cloning and functional studies of a novel gene aberrantly expressed in RB-deficient embryos. Dev. Biol. *207*, 62–75.

Zou, Y., Stoeckli, E., Chen, H., and Tessier-Lavigne, M. (2000). Squeezing axons out of the gray matter: a role for slit and semaphorin proteins from midline and ventral spinal cord. Cell *102*, 363–375.